This manuscript is the accepted version, currently in press, to be published in the Friction journal.
Submitted 6 April 2023; Submitted in the current form 27 November 2023; Accepted 18 December 2023

Methodology for the assessment of the friction torque of ball slewing bearings considering preload scatter

I. Escanciano *[a], I. Heras[a], F. Schleich[b], L. M. Macareno[a]

[a] Department of Mechanical Engineering, University of the Basque Country, Bilbao, Spain

[b] Fraunhofer-Institute for Wind Energy Systems IWES, Hamburg, Germany

*Correspoding author: Iñigo Escanciano, E-mail: inigo.escanciano@ehu.eus

Abstract: This manuscript presents an innovative methodology for the assessment of the friction torque of ball slewing bearings. The methodology aims to overcome the limitations of state-of-the-art approaches, especially when the friction torque is conditioned by the preload of the balls. To this end, the authors propose to simulate the preload scatter when solving the load distribution problem, prior to the friction torque calculation. This preload scatter allows to simulate a progressive transition of the balls from a four-point contact state to a two-point contact one. By implementing this capability into an analytical model, the authors achieve a successful correlation with experimental results. Nonetheless, and depending on the stiffness of the structures to which the bearing is assembled, it is demonstrated that the rigid ring assumption can lead to inaccurate friction torque results when a tilting moment is applied. The methodology described in this research work is meant to have a practical application. Therefore, the manuscript provides guidelines about how to use and tune the analytical model to get a reliable friction torque prediction tool.

Keywords: slewing bearing, ball bearing, friction torque, preload scatter

Nomenclature

α_0	Ball-raceway initial contact angle
β	Ball rotation angle

C	Constant parameter for the friction torque
D_w	Ball diameter
D_{pw}	Pitch diameter of the ball set
i	Number of ball rows
μ	Coefficient of friction
m	Mean effective preload
RMSE	Root Mean Square Error
MRE	Mean Relative Error
M_f	Friction torque
s	Ball-raceway contact osculation ratio
SD	Standard Deviation of the effective preload
z	Number of balls per row

1. Introduction

Ball slewing bearings are four- or eight-point angular contact bearings that are used for orientation purposes in many applications. Currently, they play an essential role in wind turbine generators, where they are used to control the yaw system (yaw bearing) and the pitch angle of the blades (blade bearings). A precise control of these components is needed to achieve the best performance of the wind turbine and this requires characterising the bearing behaviour under operating conditions. An accurate prediction model of the bearing performance is useful not only to actuate the orientation system, but also to optimize the bearing during the design process. For this purpose, the National Renewable Energy Laboratory (NREL) [1] and some bearing manufacturers [2,3] give simple and practical formulas for the estimation of the friction torque. These formulas are generic and do not consider many aspects that affect the friction torque, like the osculation ratio of the ball-raceway contact or the preload of the balls. However, they are very useful to roughly estimate the friction torque under specific load conditions. This work is focused on the analysis of the friction torque of ball slewing bearings and how to obtain more reliable estimations of this key parameter.

To calculate the friction torque in two-point angular contact bearings, there exist approaches like the one proposed by Houpert [4], where the contribution of different sources of friction are calculated separately and they are summed to obtain the total torque. Manufacturers also give similar formulas for their conventional (not slewing) bearings [5,6]. More advanced approaches have been also proposed for angular contact ball bearings, like the recent one by Zhao et al. [7]. These formulas can be applied to four-point contact bearings if they only bear axial forces, since in this case, they work like two-point angular contact bearings. However, they are not valid for ball slewing bearings, either for those with one row (four-point contact bearings) or with two rows (eight-point contact bearings). In slewing bearings, the rolling elements are usually assembled with preload (negative clearance) and bear not only axial loads, but also bending moments and radial forces. This fact affects greatly ball kinematics and the friction torque, making approaches in [4–6] not applicable. With this in mind, and on the basis of Jones's work [8] for angular contact ball bearings, Leblanc and Nelias [9,10] proposed a model to solve the load distribution and ball kinematics in four-point contact bearings subjected to any load combination, either assembled with clearances or preloaded. These approaches [8–10] assumed rigid rings and full sliding in the ball-raceway contacts. Once the load distribution and ball kinematics are known, the friction torque can be computed. Later, Joshi et al. [11] particularized the previous approach for slow-speed applications, which is mostly the case of slewing bearings. Moreover, the approach was also validated, obtaining a good correlation with the experimental results of the friction torque. Regardless of the capabilities of the approach, it presents convergence issues, which can be overcome as proposed by Heras [12]. Besides that, the friction torque of slewing bearings can also be calculated using the Finite Element Method (FEM) [13–15], although it requires a high computational cost. Nevertheless, this method allowed Heras et al. [12,14] to study the stick-slip regions in ball-raceway contacts. From these works, it was concluded that, even if the stick regions affect the shear stresses in the contacts, their effect on the friction torque is almost negligible. For this reason, it was concluded that the full-sliding hypothesis in [9–11] is acceptable when calculating the friction torque in ball slewing bearings. It is worth mentioning that, in [13], the effect of manufacturing errors in the friction torque was studied using the FEM. This research work demonstrated that, when the friction torque is conditioned by the preload, manufacturing errors can significantly affect it.

As stated before, the load distribution and ball kinematics must be known in order to make a reliable estimation of the friction torque. According to [11], assuming low speeds allows decoupling the load distribution problem and the solution of the kinematics. Therefore, the former can be solved independently, for which different approaches exist. In this regard, analytical approaches based on contact geometrical interferences can be used, like the one proposed by Aguirrebeitia et al. [16,17], where rigid rings are assumed. Other authors [13,15,18] considered the flexibility of the rings and the surrounding structures in their models. Nevertheless, due to its versatility, using the FEM constitutes the common practice to consider the flexibility of the system, regardless of the high computational cost [19–26]. In this sense, there exist different techniques to make FE models more efficient by substituting the balls by non-linear springs that simulate the flexibility of the contacts. From the research works which consider the flexibility of the system, it is concluded that it has a high impact on the load distribution. Regarding the manufacturing errors, it must be noted that they affect the friction torque insofar as the load distribution is affected by them. Some works simulate the manufacturing errors by means of analytical approaches [13,15], while others used FE techniques [27,28].

Regarding friction torque experimental data in the literature, there exist many works that perform tests with radial, axial or angular contact bearings [4,29–32]. However, there is no extensive literature on the friction torque tests with ball slewing bearings. Long et al. [33] studied the effect of the contact angle for a four-point contact bearing with clearance and under axial load, but under these load conditions, it behaves like a regular angular contact bearing. Joshi et al. [11] conducted some experimental tests for an axially loaded small-sized four-point contact bearing, considering both preload and clearances. Yet, in the preloaded case, they considered loads where the balls always had four points in contact, thus not representing what happens when the load is increased and a transition happens, where the balls switch from four to two contact points. Later, Heras et al. [34] performed experimental tests to study this transition in a small-sized ball slewing bearing. Additionally, the experimental tests were compared with the analytical results obtained using Joshi's approach [11]. The same year, Stammler et al. [35], from the Fraunhofer IWES, published a research work with normalised friction torque results obtained experimentally. Since the results were normalized, they could not be used for comparison purposes with data from other sources. The latest and more complete experimental results for ball slewing bearings were performed and published by Menck et al. [36], also from the Fraunhofer IWES. In this research work, friction torque tests were performed for three different sizes of ball slewing bearings (blade bearings), working under axial forces and bending moments.

The main goal of this manuscript is to propose an innovative methodology to predict the friction torque in ball slewing bearings. In particular, this work is focused on the transition of the contact state of the balls from four to two contact points. This transition has been observed in experimental tests [34,36] and reproduced through FE simulations [14]. Nonetheless, using current analytical formulations [11], the transition occurs abruptly for axial loads [34] and does not agree with experimental tests. Thus, to smooth the transition, in this manuscript the authors propose to consider a scatter in the preload of the balls when calculating the friction torque analytically, instead of assuming the same preload in all the balls. After proving the versatility of this proposal through a sensitivity analysis, the parameters of the model are tuned for a particular case, in order to fit experimental test results for axial load and bending moment [36]. Additionally, the effect of the flexibility of the rings and the surrounding structures on the friction torque is also studied. To conclude, different strategies are suggested to implement the proposed methodology in different case scenarios, in order to achieve the most accurate friction torque estimation model in each case.

2. Materials and methods

2.1. Problem description

Slewing bearings usually work under high loads and rotate at very low speeds. Thus, the dynamic forces can be neglected. This allows decoupling the load distribution problem and the friction torque problem. Considering this, and using the approach in [11], the solid line in Figure 1 is obtained for one of the bearings used by Menck et al. in [36]. Indeed, the figure also shows the experimental data corresponding to that bearing.

When considering the geometry of a bearing with no defects neither in the raceways nor in the balls, the analytical results do not adjust the experimental data, as it is shown in Figure 1. In this case, the analytical model has been tuned by changing the preload of the balls, so it matches the experimental results when the bearing is under no load condition, i.e. in an idling state, as it is observed in Figure 1 for an axial force of 0kN.

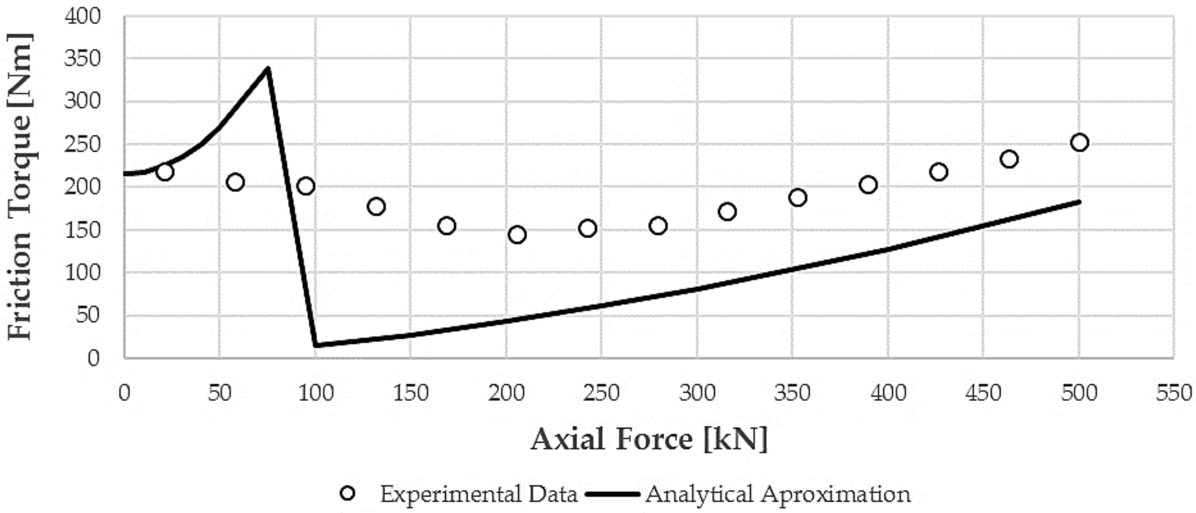

Figure 1. Friction torque experimental test results [36] and analytical tool results [34].

From the solid line in Figure 1 for the range from 0kN to 75kN, it can be guessed that the loads are distributed among the four contact points (see Figure 2a), increasing the friction torque with the applied external force. While the axial load increases, the load at two contact points increases (opposite points in one diagonal, see Figure 2a), while it decreases at the other two (the other diagonal). After a certain axial load, the load difference between the two contact diagonals is high enough, so the ball kinematics change and the friction torque decreases drastically. This can be seen in the solid line in Figure 1, for the range from 75kN to 100kN. Once the ball-raceway contact status changes to two-point contact, a further increase in the applied axial force leads to a corresponding increase in the load on these contact points, which implies higher friction torque. This can be appreciated in the solid line in Figure 1, starting at 100kN.

In practice, it is never the case that all the balls have exactly the same ball-raceway contact force in an idling state; in other words, the actual ball preload is not the same in all the balls after the bearing is assembled and before applying any load. Therefore, this initial increase of the friction torque followed by an abrupt drop does not occur in practice, as the experimental test results show in Figure 1. For a better understanding of the phenomenon, the changes in the kinematics of a ball for an increasing axial load are analysed below.

First, three zones are defined based on the evolution of the contribution of one ball to the total friction torque of a bearing subjected to an axial load (see Figure 2b). These zones are determined according to the contact status of the balls and are easily identifiable.

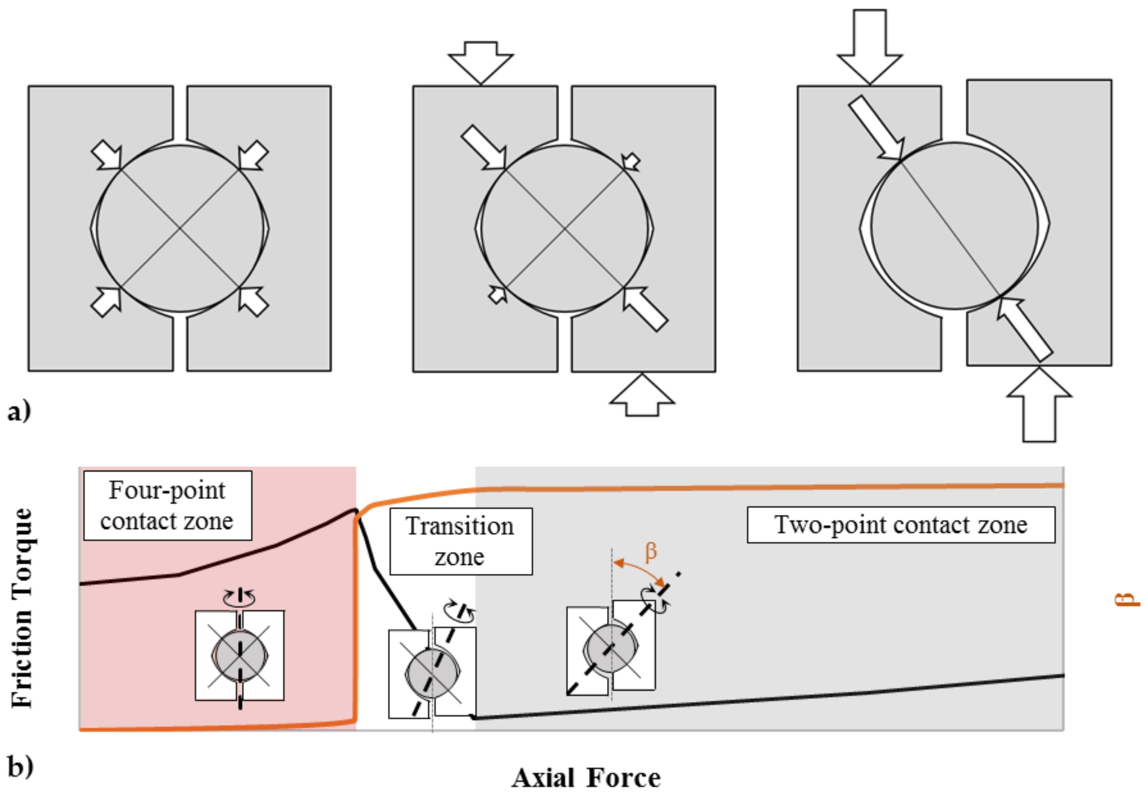

Figure 2. a) Contact loads evolution in a preloaded ball for an increasing axial load: no load (left), low-load (middle) and high-load (right). b) Friction torque curve zones definition based on the contact state of a ball.

In the first zone, referred to as the *four-point contact zone*, the axis of rotation of the ball is parallel to the axis of rotation of the bearing, so both rolling and spinning happen in ball-raceway contacts. This can be seen in Figure 2b, where the axis of rotation of the ball is represented. In the idling state, the ball has four equally loaded contact points due to the preload.

When the axial load increases, not only increases the load at two of the contact points as stated before but also affects the ball-raceway contact angle. This fact causes the angle of rotation of the ball β to change slightly in this first zone, as shown in Figure 2b. The increase of the normal contact forces in these two points involves higher frictional forces, thus increasing the friction torque. At the same time, the load at the other two contact points decrease, together with the rolling component at these points, and increases the spinning component, which also has an influence on the increase of the friction torque.

In the second zone, called the *transition zone*, two of the contacts have already lost a large part of their load. This fact makes the two most loaded contact points change to a rolling state without almost any spinning, so that the axis of rotation of the ball is almost perpendicular to the dominant contact diagonal. This change in the kinematics causes a drop in the contribution of the ball to the friction torque of the bearing (see Figure 2b).

Finally, in the area referred to as the *two-point contact zone*, the previously less loaded contacts become completely unloaded, leaving the other two to support the entire applied load. In this area, the contribution of the ball to the friction torque of the bearing increases with the axial load as seen in Figure 2b.

After analysing the kinematics of one ball, the drop in the analytical approximation of the friction torque for the entire bearing can be justified, for an axial load (solid line in Figure 1). The point is that, if all the balls in the bearing are subjected to the same conditions, they will experience the same evolution as the one in Figure 2b, simultaneously. Thus, the drop that happens for one ball is reproduced in the whole bearing. Contrarily, the experimental results (see experimental results in Figure 1) show a smooth evolution of the friction torque with the applied axial load. This observation can be justified if we assume that the balls gradually move from four to two contact point state, but not at the same time. This gradual transition can be caused because, in practice, the actual preload is not the same for all balls. Figure 3 shows how different ball preloads cause the transition to occur at different points, according to the analytical approach. Therefore, having different preloads in each ball, will cause the transition of each one to happen for a different axial load, thus smoothening the drop observed in the friction torque of the whole bearing.

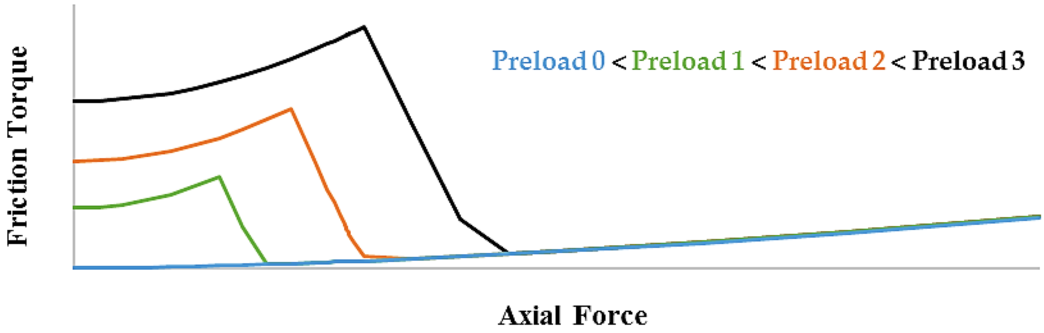

Figure 3. Contribution to the friction torque of a ball for different preload levels.

Finally, the difference in the friction torque in the two-point contact zone between analytical results and experimental data is almost constant in Figure 1. This could be due to the effect of different elements, like the seals or the cage, acting as a constant source of friction torque. The constant effect of these elements can be seen in the experimental results of [36], where a bearing was disassembled to remove the seal and its contribution to the frictional torque was found to be almost constant.

In short, the difference in the actual preload of the balls can justify the mismatch between the analytical and experimental results. Therefore, this is adopted as the main hypothesis on which the method presented in this paper is founded. In this regard, two main factors may account for the difference in the actual preload of the balls: the manufacturing errors of the raceways and the assembly process of the bearing to the surrounding structures. On the one hand, raceway manufacturing errors alter the preload of the balls, which causes some of them to be more or less loaded than expected (or even have clearances). Meanwhile, the manufacturing errors of the balls are almost negligible, as they are measured and classified. On the other hand, due to the flexibility of the rings, the preload level of the balls may vary caused by the bolt-tightening process [23], when assembling the bearing to the surrounding structures. Besides, the load distribution can be affected by the lack of axisymmetry of those structures.

2.2. Proposed approach

According to the presented hypothesis that explains the lack of accuracy of the analytical approach, in this paper, the preload is proposed to be simulated by means of a statistical distribution. This aims to solve the limitations of the analytical approach, described in the previous section. The details regarding this approach and the implementation of the preload scatter are given in Section 2.3.

This work consists of a series of successive works that are explained below. The following points also offer a general overview of the manuscript, describing the content of each section:

- In order to test the capabilities of the proposed approach to reproduce the experimental results, a sensitivity analysis is performed to study the influence of the statistical distribution parameters on the evolution of the friction torque. The effect of other parameters is also studied. This study is described in Section 3.
- From the results of the previous study, a procedure is presented to tune the analytical model in order to fit the experimental data obtained by Menck et al. [36]. This procedure is explained in Section 4, where the main results of this manuscript are presented.
- The effect of the flexibility of the rings and the surrounding structures is studied through finite element analyses (FEA). This effect is especially relevant in the case of an applied bending moment, as can be seen in Section 5.
- Finally, from all the previous results, different strategies are suggested to apply the proposed approach in different case scenarios. (See Section 6)

2.3. Description of the analytical model

As introduced in Section 2.1, the calculation of the friction torque for ball slewing bearings involves two consecutive stages. The first stage consists in estimating how the load is distributed among the individual ball-raceway contacts (load distribution problem). The second stage involves calculating the friction torque as the sum of the friction torque contributions provided by each ball under the previously calculated load state (friction torque problem).

For the load distribution problem, the model used in this research work considers only the local deformations in the contact areas and does not account for the global deformations of the rings; i.e. rigid rings are assumed. Since the stiffness of the bearing rings and the adjacent elements will differ from one application to another, this assumption is adopted not only for simplicity but for the generality of the approach. Thus, the contact interference model in [17] is used, which accounts for the contact angle variation and the ball preload. Furthermore, the preload used in this study, defines the load state of the balls after the bearing assembly process, which from now on will be called "effective preload". Thus, this "effective preload" accounts for manufacturing errors and ring deformations during the assembly process, in concordance with [34].

For the implementation of the preload scatter, the model is provided with the capability of defining the effective preload of each ball independently. In this work, the different values of the preload in the bearing follow a normal distribution, since manufacturing errors are basically random. The normal distribution is defined by two parameters, the mean value (*m*) and the standard deviation (*SD*). In addition, the statistical distribution needs a seed number (*seed no*.) to be chosen for the Random Number Generation (RNG), which for traceability purposes will remain constant.

For this stage, the inputs needed for solving the load distribution problem consist of the geometrical parameters, the statistical parameters that define the effective preload (*m*, *SD*, *seed no*.) and the applied external loads. The geometrical parameters involve the ball diameter D_w, the bearing mean diameter D_{pw}, the osculation ratio of the contact s, the initial contact angle α_0, the number of balls per row z and the number of rows i. The outputs of the load distribution problem are the contact loads and contact angles for each ball-raceway contact point.

On the other hand, the friction torque problem depends on the mentioned outputs from the load distribution model. The model used for this purpose in this work is mainly based on the approach presented by Joshi et al. [11]. Once the problem is solved, the kinematics are known and the shear stresses in each contact can be computed, which allows calculating the friction forces and the contribution to the friction torque of each ball independently. The model used in the current work also implements the strategies proposed by Heras [12] to solve the convergence problems in [11]. According to the latter research, full sliding is considered in the current work, since considering regions in adhesion gives almost identical results regarding the friction torque and has a higher computational cost.

The model also considers an independent constant parameter C that is directly summed to the friction torque result. This constant allows adjusting the friction torque curve when the shape of the analytical results fits the experimental data, but an offset exists, like in Figure 1. Therefore, for solving the friction torque problem, the input parameters needed consist mainly of the contact loads and contact angles for each ball-raceway contact point (which are the outputs after solving the load distribution problem), the coefficient of friction (μ) and also some geometrical data (D_w, D_{pw}, s); the main output, in this case, is, of course, the friction torque. Figure 4 summarises the calculation stages and their inputs to obtain the bearing friction torque for the analytical model.

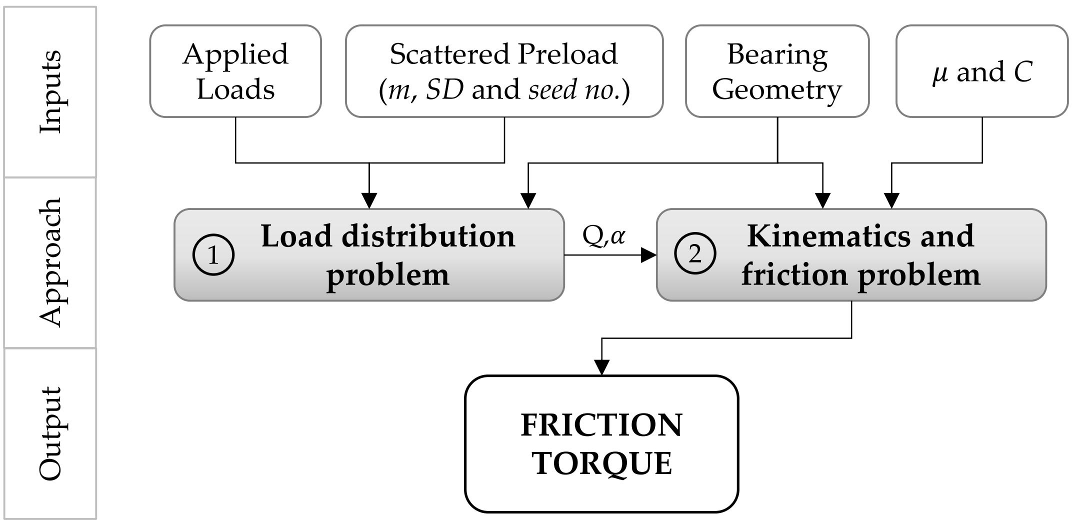

Figure 4. Calculation stages of the analytical model.

2.4. Studied case

As explained in Section 2.2, the analytical model will be tuned to fit already existing experimental data in [36] in order to check the capabilities of the proposed approach to reproduce the real evolution of the friction torque, especially in the transition zone. The data of the geometry of the bearing tested in [36] is summarised in Table 1.

Table 1. Bearing geometrical data.

Symbol	Value		Symbol	Value
D_w	25.4 mm		α_0	45°
D_{pw}	673 mm		z	69
s	0.94		i	2

It must be noted that in [36], the bearings were tested in pairs, and the measured friction torque was divided by two for the plots. Conversely, in the current work, the total friction torque corresponding to both bearings is represented when studying the results. Moreover, the names of the experimental results used in this paper are renamed according to Table 2 to maintain a clearer schema of the results.

Table 2. Experimental dataset names corresponding to the bearing pairs used for the experimental tests.

Bearing pair [36]	**Experimental dataset name (this manuscript)**
143 and 144	Experimental data 1
172 and 173	Experimental data 2
162 and 163	Experimental data 3
174 and 175	Experimental data 4

Considering the data that is known for this case, the tuning parameters that will be used to adjust the analytical model to experimental results are selected accordingly, and in concordance with the proposed approach. Therefore, the tuning parameters will be:

- The statistical distribution parameters that define the effective preload (m and SD): manufacturing errors are unknown and the effect of the assembly process on the effective preload cannot be directly calculated.

- The coefficient of friction (μ): reference values are known from the literature [11,32,34], but it is unknown for this specific case. The considered values when tuning the model must be near the ones in the references.
- The independent constant (C): the effect of the phenomena related to this parameter (seals, cage, etc.) cannot be directly estimated.

Therefore, according to the defined tuning parameters, the friction torque will be calculated as follows, based on the analytical approach described in this section:

$$M_f = f(m, SD, \mu) + C$$

3. Study of the parameters

In this section, a sensitivity analysis of the tuning parameters selected in Section 2.4 for the studied case is presented. The influence of these parameters in the evolution of the friction torque is therefore studied when using the analytical procedure described in Section 2.3.

3.1. Statistical distribution parameters

In this section, the influence of *m* and *SD* in the studied case (see Section 2.4) is studied. Figure 5a shows the effect of *SD*. It can be seen that in the transition zone (50kN - 100kN), the case with no deviation of the effective preload (*SD* = 0μm) shows a sharp variation of the friction torque. The plot shows how this sharp variation can be smoothed by introducing a deviation to the effective preload distribution. It can be seen that, as the value of the standard deviation increases, the idling friction torque becomes higher. Furthermore, due to the smoothed behaviour of the transition zone, the beginning of the two-point contact zone occurs for higher axial loads. For the case with zero standard deviation, this occurs for an axial force of 100kN; for higher values of the standard deviation, the two-point contact zone starts for axial forces in the range of 150kN to 300kN, for the considered cases. Finally, once the two-point contact zone is reached, the friction torque does not vary significantly with the standard deviation.

If the influence of *m* is analysed, as shown in Figure 5b, a similar effect is observed. Hence, the higher *m* is, the higher the idling friction torque becomes. In addition, the friction torque requires a higher axial load to reach the two-point contact zone. As it happened with *SD*, *m* does not affect the friction torque once the two-contact point zone is reached.

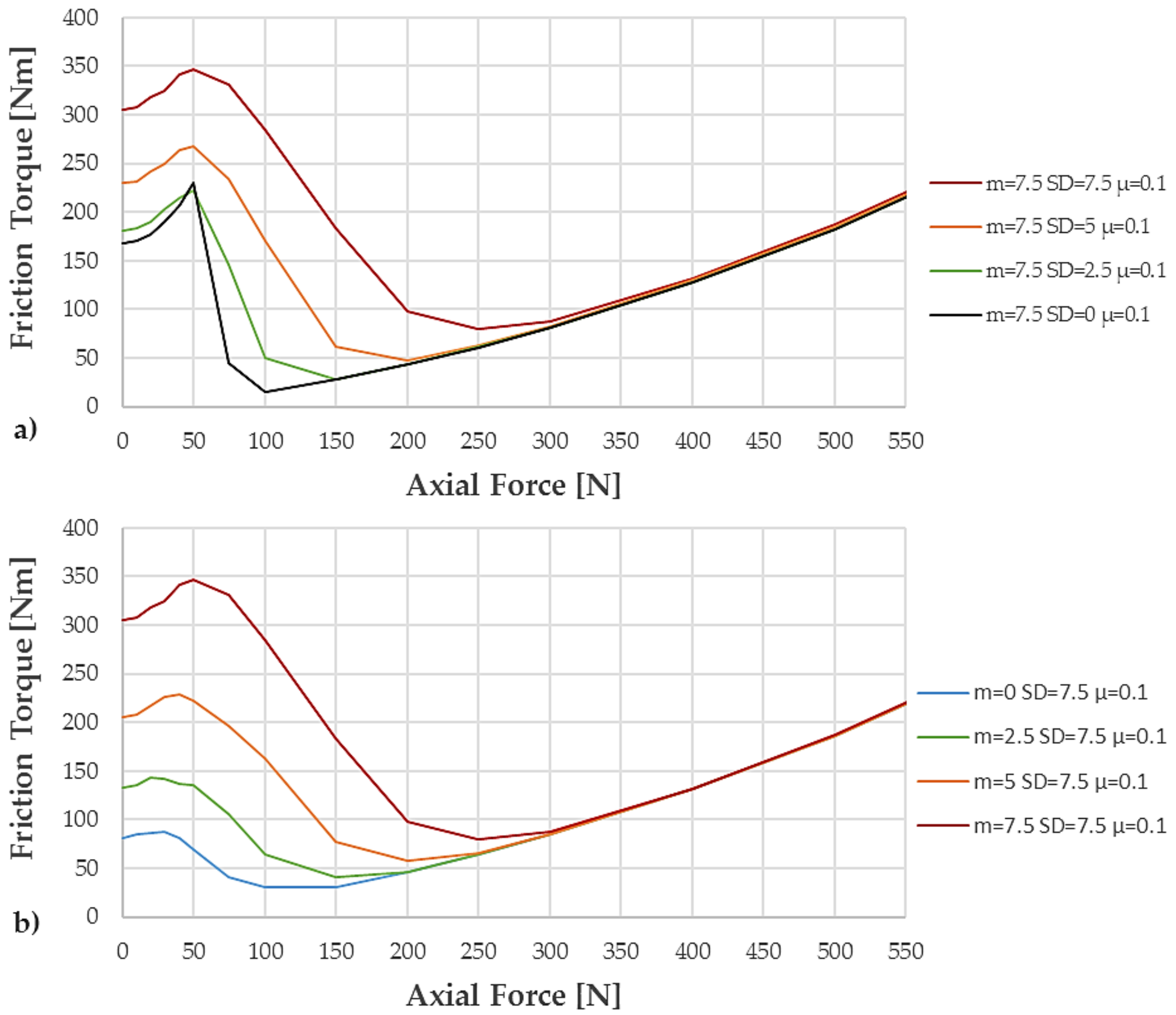

Figure 5. Effects of the standard deviation of the effective preload for constant mean preload m = 7.5µm on the friction torque analysis (a). Effects of the mean effective preload for constant standard deviation SD = 7.5µm on the friction (b).

In the following, the effect of different seeds for the statistical distribution of the effective preload is analysed. The *seed no.* affects the random number generation, which means that affects the scatter of the effective preload. Changing the *seed no.* has a similar effect to changing the order of the balls inside de bearing or rotating the bearing. When a bearing is subjected to a pure axial load, the azimuthal position of a preloaded ball does not affect the fraction of the applied load it has to bear. Therefore, the effect of changing the *seed no.* on the bearing friction torque would be negligible under an applied axial load. However, this does not happen for load cases involving radial or moment loads. Figure 6 shows the effect of the *seed no.* for the case of an applied bending moment. The result of varying the seed number causes a minor change in the absolute value of the friction torque, without almost varying the shape of the curve. However, a greater effect could take place for different *seed no.* than the ones shown in this example, or for different conditions (load or geometry). As an example, let's consider that the most preloaded balls turn out to be in the area that has to face a small fraction of the applied load. In this case, they remain in the four-point status even for high applied loads. Therefore, and being their preload high, their contribution to the friction torque will be also high.

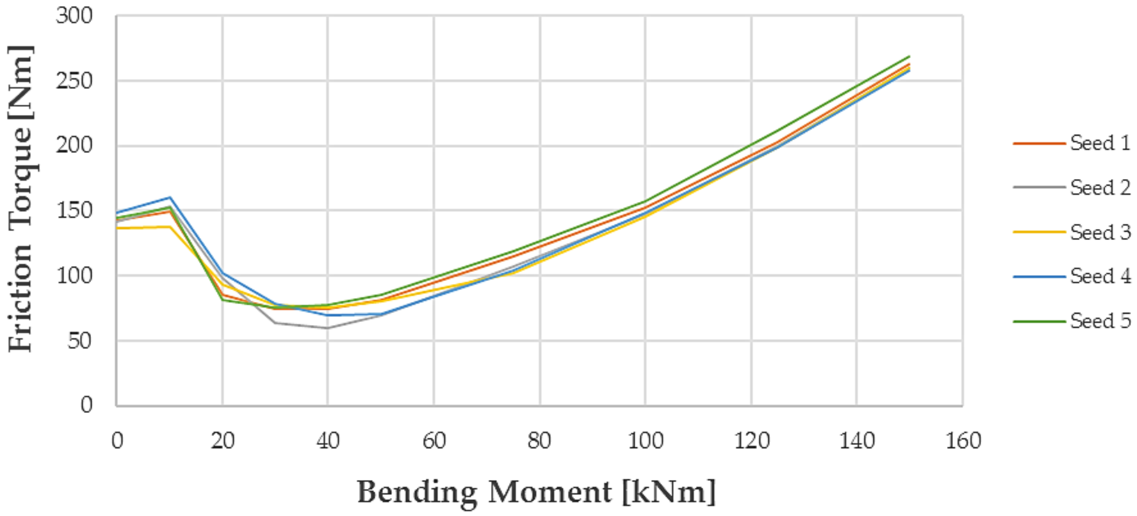

Figure 6. Analysis of the seed selection for random number generation on the friction torque analysis.

Therefore, after analysing the effect of the statistical distribution parameters, it can be stated that the preload scatter implies noticeable changes in the evolution of the friction torque of a ball slewing bearing. Moreover, the effect smooths the four-point to two-point contact transition, in line with what is observed in the available experimental results. Therefore, it is reasonable to expect a better correlation between the analytical model calculations and the experimental data by considering this preload scatter.

3.2. Coefficient of friction and independent constant

Figure 7a shows the effect of varying the coefficient of friction on the friction torque. As expected, the coefficient of friction affects the friction torque proportionally. Accordingly, the axial load required to reach the two-point contact zone remains the same as the coefficient of friction changes (150kN for *m*=5µm, 60kN for *m*=0µm, see Figure 7a). Furthermore, it is observed that the two-point contact zone remains unaltered for different values of *m* with the same coefficient of friction. Lastly, the constant parameter *C* introduces an offset to the friction torque, as shown in Figure 7b.

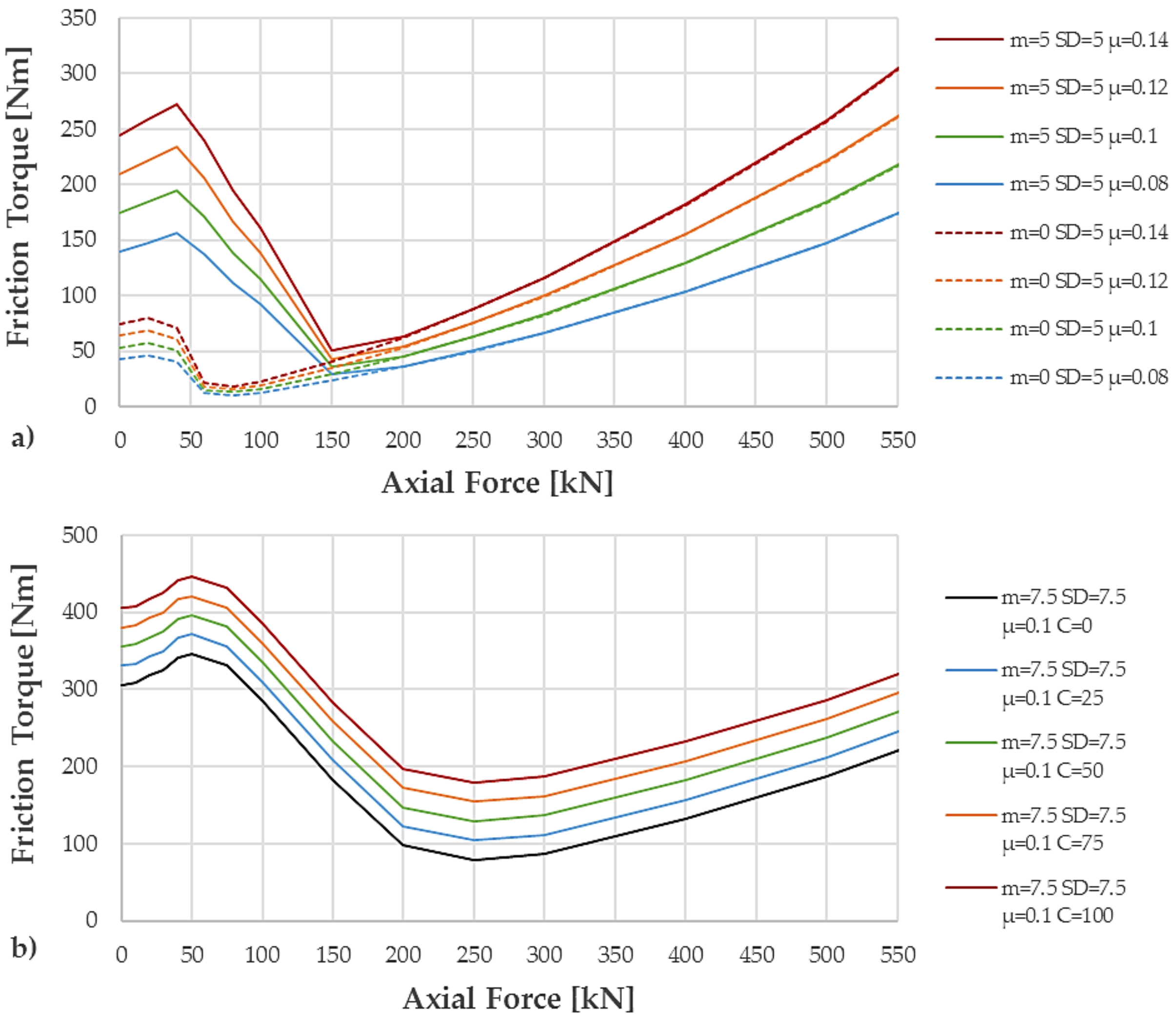

Figure 7. Effects of the coefficient of friction (µ) on the friction torque analysis (a). Effects of the constant (C) on the friction torque analysis (b).

From these analyses, it is concluded that, among the studied parameters, only two of them affect the friction torque on the two-point contact zone: μ and *C*. The first one affects the slope of the curve, while the second one only introduces an offset to the curve. On the other hand, *m* and *SD* have been proven to greatly affect the four-point contact zone and the transition zone, smoothening the drop of the original approach by [11]. Therefore, introducing the ball preload scatter gives the analytical model the capability to better fit the experimental results, which is the goal of this research work.

4. Approximation to experimental results

The purpose of this section is to check the capability of the proposed method to reproduce experimental measurements. With this aim, several analyses were performed considering different combinations of the tuning parameters to achieve a good correlation with the available experimental data [36]. From now on, only the results relative to *Experimental Data 1* are shown (see Table 2), but the procedure in this section was repeated for every experimental data set, whose results are summarized at the end of this same section.

4.1. Experimental setup

The experimental friction torque results used for the model approximation in this paper are obtained with the Fraunhofer IWES test rig BEAT1.1 (Bearing Endurance and Acceptance Test rig) which is shown in Figure 8.

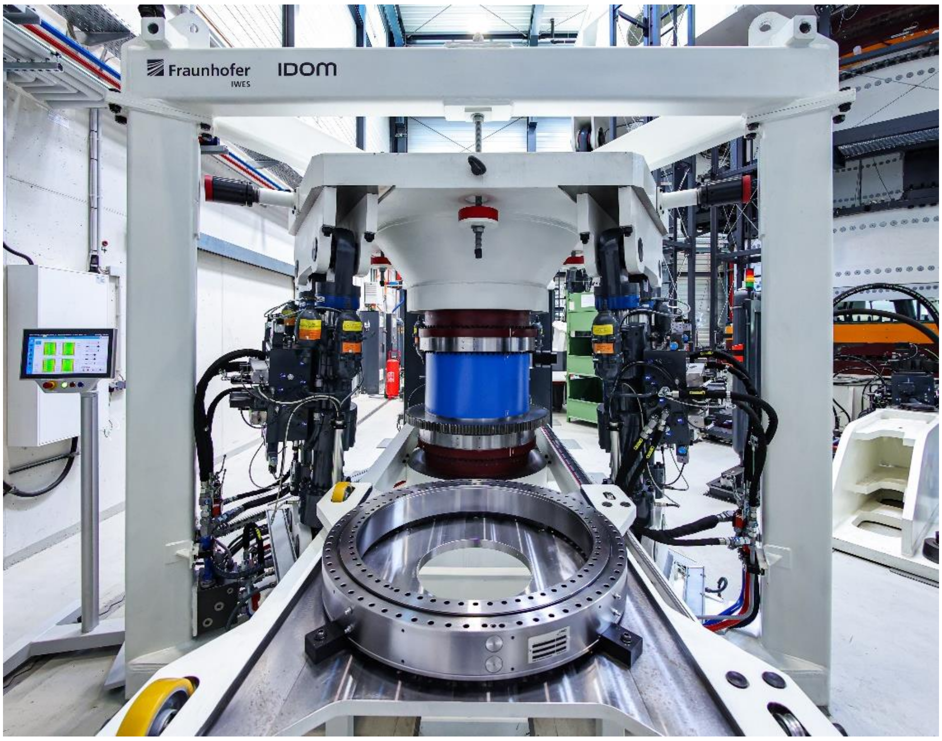

Figure 8. BEAT1.1 test rig with exemplary test bearing (©Fraunhofer IWES/Ulrich Perrey)

Six hydraulic actuators in hexapod configuration connect to a load platform on top and enable a complex load application in six degrees of freedom. Two eight-point contact ball bearings (i.e. two double row four-point contact bearings) with the properties in Table 1 are tested simultaneously. An electric pitch drive introduces the pitch movements by a gear connection with a pinion and geared ring. The friction torque is measured for both bearings together by a calibrated torque meter located between the gearbox and the electrical drive. Due to this position for the measurement, the torque of the gearbox needs to be subtracted, which is done by an empirical function developed by IWES [36]. The friction torque results used for the following model approximation procedure are obtained with pure axial force and pure bending moment tests. The measurements were done for 30 different load levels in the ranges of -200kN (tension) to +500kN (compression) for the axial load, and -125kNm to +125kNm for the bending moment. Due to the limited capacity of the bearings' bolted connection, the maximum tension force is lower than the compressive force for the axial load tests.

4.2. Procedure

The procedure to adjust the analytical model consists of searching for a set of values of the tuning parameters that best fit the experimental data. Firstly, this task is performed for the axial load case, since the different contact state zones (see Figure 2b) can be more clearly identified under these working conditions. This happens because, under an applied pure axial force, the load is distributed almost equally among the balls, and there is a point from which the two-contact zone is reached for every ball. Therefore, the values of the tuning parameters that best fit the axial experimental results are defined in the first place. Then, these values are used to check the correlation with the bending moment case.

First of all, from the study of the coefficient of friction, it was concluded that it is the only parameter that affects the slope of the friction torque curve in the two-point contact region (see Figure 7a). Thus, it is selected as the first parameter to be tuned. In order to identify if a point from the experimental data is part of the two-point contact region, the slope of the curve is analysed. When the friction torque starts to increase steadily, it can be considered that the bearing is in the two-point contact zone (see Figure **9**). The adjustment procedure of this parameter consists of looking at the slope of the curve in this zone.

The coefficient of friction that best fits the slope of the experimental results is therefore selected. The Root Mean Square Error (RMSE) is used for this purpose, which is calculated according the following formula, where n is the number of points considered for the curve fitting:

$$RMSE = \sqrt{\frac{1}{n}\sum_{i=1}^{n}\left(T_i^{analytical} - T_i^{experimental}\right)^2}$$

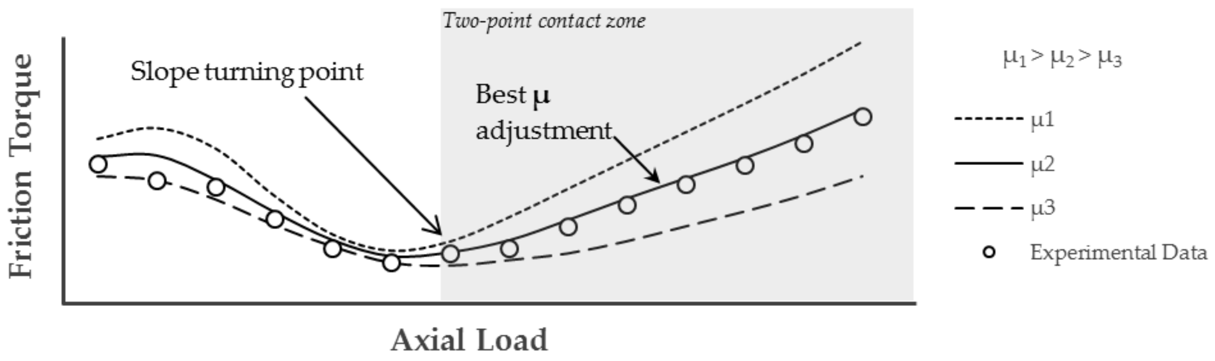

Figure 9. Example schema of the selection procedure for the coefficient of friction.

Subsequently, multiple analyses are performed by varying *m* and *SD*. With these analyses, different curves of the friction torque are obtained. For each curve, *C* is adjusted to minimise the RMSE in the two-point contact zone. The curves with less Mean Relative Error (MRE) in relation to experimental results are selected, and consequently, the combinations of values for the tuning parameters. The MRE can be expressed as follows:

$$MRE = \frac{1}{n}\sum_{i=1}^{n}\frac{\left|T_i^{analytical} - T_i^{experimental}\right|}{T_i^{experimental}}$$

The described procedure was followed to analyse the analytical results of the friction torque of the studied bearing under axial load and bending moment, separately. The results are compiled and discussed in the following section.

4.3. Results and discussion

As pointed out above, the results in this section only include the *Experimental Data 1* dataset and they are divided into two sub-sections: axial load case and bending moment case. Then, the results are summarised for the rest of the cases.

4.3.1. Axial load

Following the described procedure, a coefficient of friction of 0,085 was found to best fit the experimental results. Then, calculations were made considering different combinations of *m* and *SD*. Figure 10 shows the MRE of the analytical approach concerning the experimental data for all the considered combinations. Remember that the *C* constant is calculated for each case to minimize the RMSE. The figure shows that the higher the mean value of the preload is, the lower the value of the standard deviation that retrieves a good fit (a low error). When performing the sensitivity analysis in Section 3, it was observed that the effect of both parameters, *m* and *SD*, was qualitatively very similar. In this sense, the results in Figure 10 are coherent with this observation. Note how the cases with the lowest errors are organized in a band form in the heatmap. So, there is not only one combination of these two values that best fit the experimental results but a set of them.

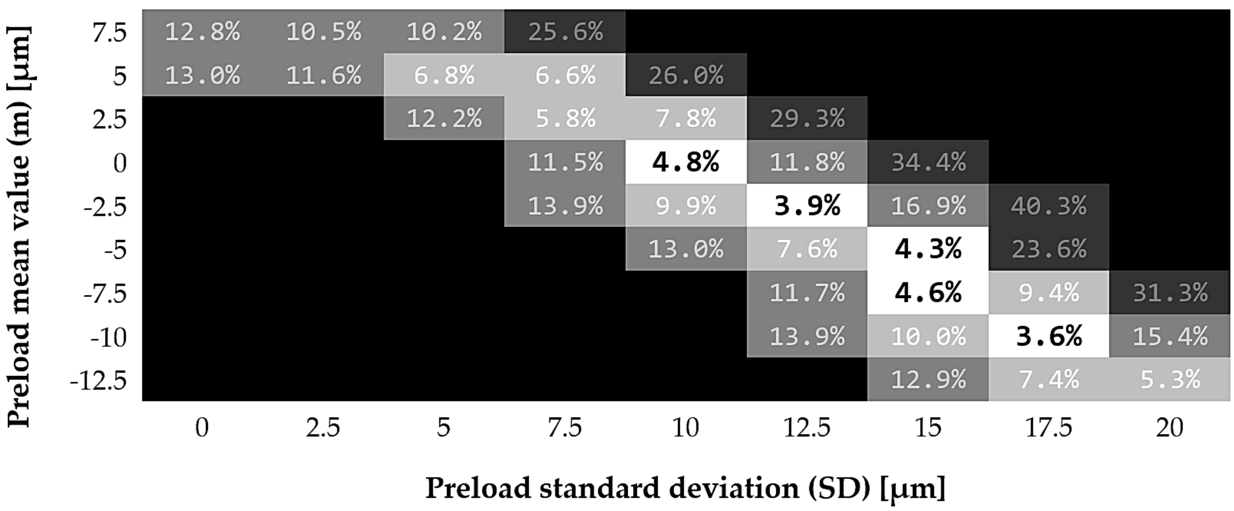

Figure 10. MRE heatmap for different combinations of *m* and *SD*.

Figure 11a shows the friction torque curves corresponding to the values of *m* and *SD* that retrieve an error lower than 5%, according to Figure 10. In this figure, both compression and tension load cases are represented, corresponding to negative and positive values of the axial load, respectively. On the compression side, analytical results show a good match with the experimental data. Note how the curves meet once all the balls are in the two-contact zone, where the effect of the preload is already negligible. On the tension side, analytical results are symmetric because, under the rigid rings assumption, the load distribution is the same, thus leading to the same friction torque. The results show also a good correlation for the tension side, except for one experimental data point. The lack of experimental results for higher tension loads prevents reaching further conclusions in this regard.

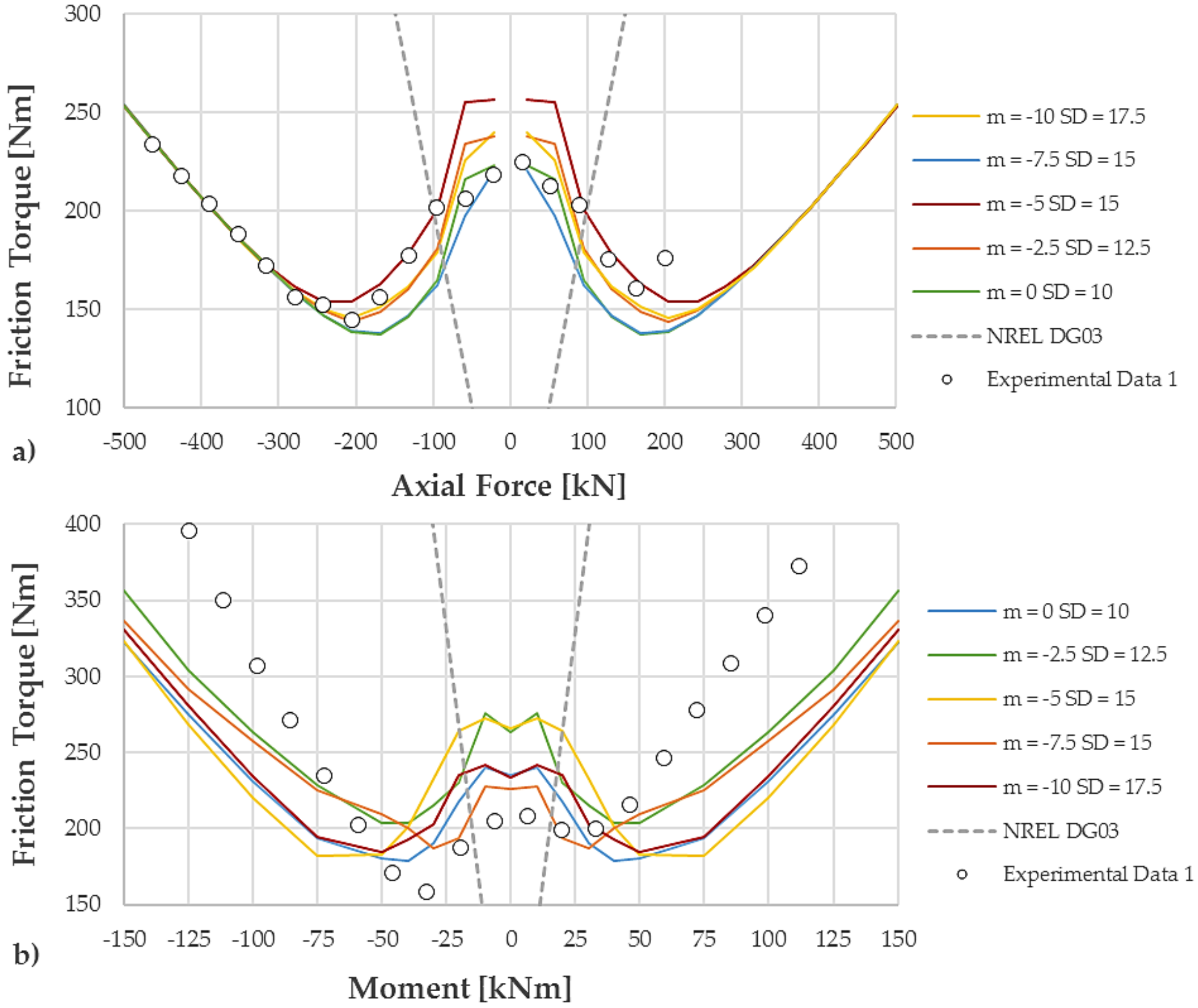

Figure 11. Analytical results selection adjusted to experimental results under axial load (a) and bending moment (b).

Figure 11a also includes the results according to the formula proposed by the NREL in their design guideline [1]. It can be observed how, coherently with the guideline, the estimated friction torque is overestimated for high axial loads. Nonetheless, for light loads, the friction torque is largely underestimated by this formula. In this regard, the proposed approach is demonstrated to be far more accurate.

4.3.2. Bending moment

Once the values for the parameters μ, m, SD and C that retrieve the lowest error for the axial load case were obtained, they were used to perform calculations for an applied bending moment. The results are shown in Figure 11b. The sign of the bending moment defines the direction of the applied load. As it happened in the axial load case, and due to the rigid ring assumption, the analytical approach retrieves the same results for both positive and negative bending moments. This symmetry is not observed in the experimental results, which can be explained by the ring deformation behaviour of the test bearings. If the flexibility of the rings and the structures of the test bench affect the load distribution, it will also affect the friction torque, which would explain not only the lack of symmetry of the test results, but also the poor correlation between the analytical approach and the experimental results. Therefore, even if the current approach is far more accurate than the formula from the NREL [1], it cannot be considered a satisfactory match. This fact leads to the following section (Section 5), where the effect of the flexibility of the rings and the structures is considered.

4.3.3. Results summary for all the cases and discussion

The described procedure was repeated for the rest of the experimental data as listed in Table 2. Table **3** contains the ranges for the values of the tuning parameters (maximum and minimum values) that best fit each experimental dataset (see Table 1), with a MRE of less than 5%. The first row in Table **3** correspond to the bearing pair studied above (see Figure 11a, note that the values in the legend are in agreement with Table 3). The coefficient of friction is always in the range of 0.085 and 0.11, which is coherent with [11,31,32,34,37–39]. Since each experimental data corresponds to different bearings, mounted with balls of slightly different sizes, the mean effective preload *m* is coherently different in each case. Nonetheless, all the bearings were provided by the same manufacturer, so the manufacturing errors are expected to be similar in every case. Moreover, they have been mounted in the same test bench, and assembled following the same procedure. Coherently, the standard deviation of the effective preload *SD* is very similar in every case, and always in the range of 7.5µm and 17.5µm. Note that a good fit can be achieved with a negative value of *m*, which means that more than half of the balls will have a clearance (not preloaded). Finally, the value of the constant C is in the range of 73Nm and 123Nm, which means that this parameter has a great effect on the friction torque.

Table 3. Values of the tuning parameters for the different experimental tests.

	μ	m [μm]	SD [μm]	C [Nm]
Experimental data 1	0.085	[-10, 0]	[10, 17.5]	[81,92]
Experimental data 2	0.11	[5, 7.5]	[10, 12.5]	[73,79]
Experimental data 3	0.09	[-7.5, 5]	[7.5, 17.5]	[96,113]
Experimental data 4	0.085	[-2.5, 0]	[15, 17.5]	[114,123]
Overall	[0.085,0.11]	[-10, 7.5]	[7.5, 17.5]	[73,123]

5. Effect of the deformations of the rings on the friction torque

According to the reasoning in the previous section, the deformations of the rings could be the reason for the poor correlation between the estimation of the friction torque by the analytical approach and the experimental results for the case of an applied bending moment. Previous works [13,15,18,21] showed that, for this load case, the rigid rings assumption can lead to fewer balls in the four-point contact zone, compared with the results when the flexibility of the rings and the structures are considered. Since the contribution of each ball to the friction torque is higher in the four-point contact zone than in the two-point contact zone (see Figure 2b), this can be one possible cause of the unsatisfactory analytical-experimental correlation (Figure 11b). In this section, a FE analysis is performed to check the influence of the flexibility of the rings and the surrounding structures on the resulting load distribution and thus the friction torque for the studied case under an applied bending moment. The results are compared with those from the analytical approach, where the rigid rings assumption is considered.

5.1. FE simulations

FE structural simulations of the test bench were performed to analyse the deformation behaviour of the bearing rings when a bending moment is applied. For this purpose, a FE model of the BEAT1.1 assembly, including the two mounted bearings, is developed in ANSYS Workbench. A cross-sectional view of the FE model of the BEAT1.1 with implemented bearings is shown in Figure 12.

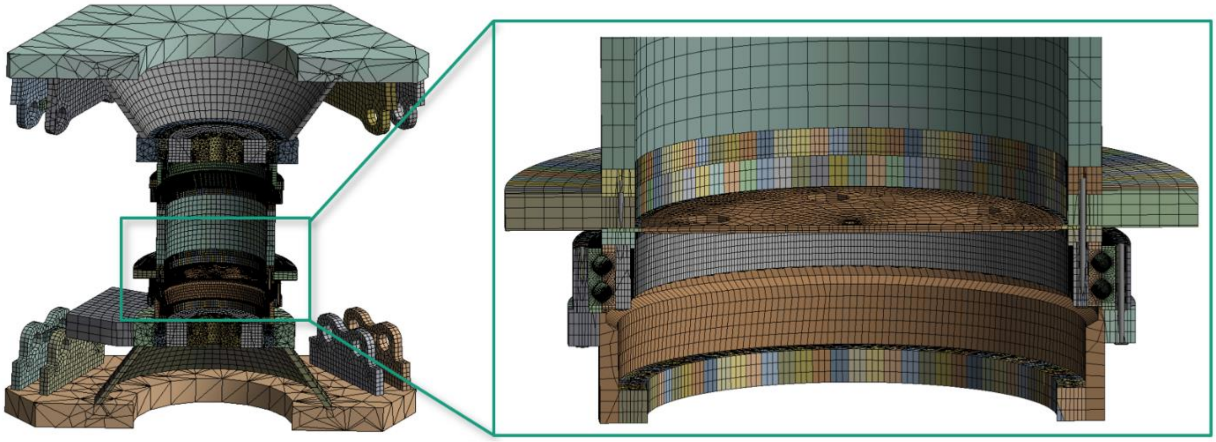

Figure 12. Cross-sectional view of the BEAT1.1 test rig FE model [36].

The two identical bearing models are generated by the use of a CADFEM extension called “Rolling Bearing inside ANSYS”. This tool for the ANSYS workbench environment implements nonlinear spring elements between the bearing rings to represent the nonlinear contact behaviour between the ball and raceway and generates a highly efficient global FE model (similarly to [19]). As the test bearings are manufactured with a preload to ensure every ball is in contact in a non-loaded condition, a constant initial ball oversize of 35 µm is also considered in the model. Bolts and frictional contacts at the flange surfaces are implemented to represent the bolted connections and to enable a realistic deformation behaviour of the structure. The different kinds of load to achieve the desired load level of the bearing are applied in a certain sequence which is illustrated in Figure 13.

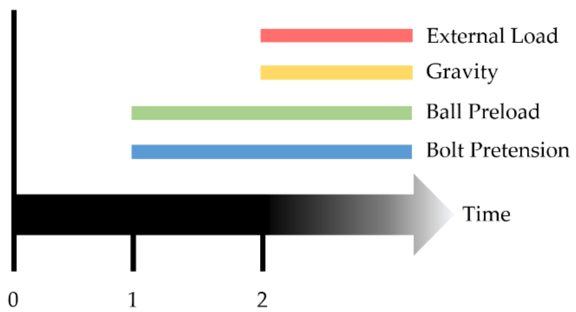

Figure 13. Loading sequence for BEAT1.1 FE simulations.

It is important to point out that this FE model will account for the flexibility of the structures, but will not simulate the main sources that cause the ball preload scatter, that is to say: 1) manufacturing errors are not considered; and 2) the bolt tightening procedure is simulated in a single load step, where all the bolts are evenly preloaded at the same time. Of course, in the real assembly, the bolts are tightened one by one and according to a specific sequence, in order to overcome the elastic interaction. Nonetheless, and even if these effects are not simulated, the contact deformations before applying the external load (what the authors call the effective preload) will not be exactly the same in every ball, as the structures will deform after the first load step.

Figure 14 shows cross-sectional views of the deformed rings of the lower test bearing loaded with a pure bending moment of 125kNm. It turns out that, even if the structure is cyclically symmetric in the surroundings of the bearings (the frame is not, see Figure 8), the bearing deforms differently on the tension (right) and compression side (left). The radial displacements on the tension side are significantly higher than on the compression side. In turn, this characteristic ring deformation behaviour leads to different contact forces and angles on both sides. On the compression side, the contact forces distribute more evenly on both rows and the resulting contact angles are less as the ring tilting is less compared to the tension side, which encounters higher contact angles. This leads us to confirm that, when a pure compression load is applied, the rigid ring assumption can be acceptable. On the contrary, for the case of axial tensile force, the raceways will “open” (see Figure 14, right), affecting the load distribution, and so the rigid rings assumption will not offer accurate results. This different behaviour under compression and tension loads also explains the lack of symmetry in the experimental results of the friction torque shown in Figure 11a for the case of an applied axial load, even if more measurements would be required in the tension side to further confirm this observation.

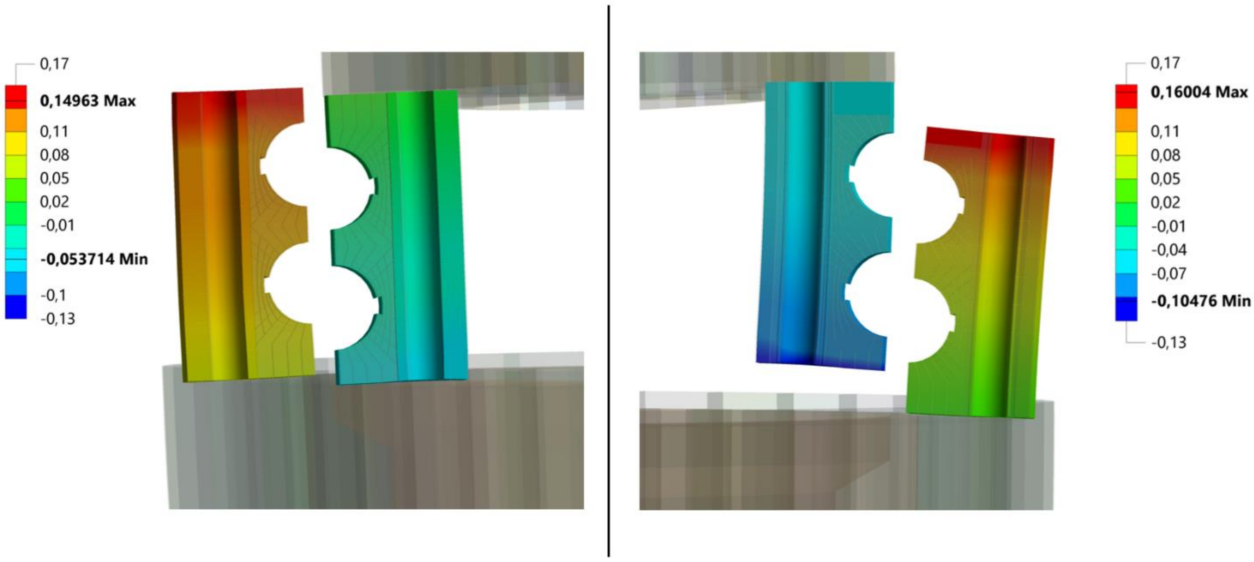

Figure 14. Radial nodal displacements of the rings in mm for M=125kNm, compression side (left) and tension side (right) in the lower bearing, Scale 50.

Furthermore, the FE simulations reveal that both test bearings are not exactly loaded in the same way. This is caused by minor differences in the surrounding structures for both bearings and shows the sensitivity of the bearing's internal load distribution towards the stiffness of the surrounding structures. As the experimental friction torque is measured for both test bearings, it is also important to consider the load distribution and contact angle evolution data of both bearings for the approximation procedure. The FE simulations are conducted with a high number of substeps to calculate the resulting load and contact pressure distributions as well as the contact angle evolutions in both bearings for several different load levels. This extensive data set is used for the following calculations.

5.2. Results and discussion

To study the effect of the flexibility of the rings and the surrounding structures on the friction torque, the load distribution results from the previously described FE analysis were extracted for each substep. Then, this data was used to feed the analytical model for the friction torque calculation. In other words, and going back to Figure 4, the analytical model for the load distribution calculation that considered rigid rings was substituted by the FE model, while the friction torque calculation was performed by the same analytical approach. As stated when describing the FE model, in this way we are able to simulate the flexibility of the system, but not the sources that cause the preload scatter, even if the effective preload is not exactly the same in every ball. The results from these calculations, identified with the name of *FEM-Analytical* in Table 4, are represented with a black line in Figure 15. The results show a very good correlation with experimental tests for loads from around 80kNm onwards, while the curve is completely different under 40kNm. Therefore, two main conclusions arise from this comparison. Firstly, and looking at the good correlation for high bending moments, it can be stated that the flexibility of the structures must be considered when calculating the load distribution to achieve accurate estimations of the friction torque. This does not mean that the analytical approach is not practical. The conclusion in this regard is that the more flexible the structures are, the less accurate estimations the approach will give. Secondly, and looking at the poor correlation for light loads, it can be concluded that the sources that cause the preload scatter must be considered if accurate results of the friction torque are required for light loads, where the effect of the preload is high. In many applications, the slewing bearings mostly work under this loading regime, so the effect of the effective preload scatter may be more relevant than the effect of the flexibility of the structures in these cases.

To confirm these conclusions, and in order to have appropriate references to compare with the new curve (the *FEM-Analytical*), the results from the FE model were used to perform two more analyses. These analyses are described below and listed in Table 4 as *Analytical 1* and *Analytical 2*. In both analyses, the load distribution problem was solved analytically and consequently based on the rigid ring assumption, i.e. as described in Section 2.4 and as was done in Sections 3 and 4. The difference is that, in the new calculations, the value for the effective preload was obtained from the FE model, instead of considering a preload scatter based on a normal distribution. This way, it will be possible to compare the analytical approach with the new *FEM-Analytical* curve, considering a similar state in the idling conditions (with no applied load). It must be noted that, when the ball preload (ball oversize) is applied in the first step of the *FE* simulations, rings are deformed, so the effective preload, i.e. the actual ball-raceway deformations before applying the external load, will be lower than the ball oversize.

The simulations in *Analytical 1* consist of applying the same effective preload throughout all balls. This preload was calculated as the mean value of all the ball-raceway deformations extracted from the *FE* analysis after the first load step (see Figure 13), i.e. the effective preload according to the FE simulation. With this unique value for the preload, the load distribution and the friction torque were calculated analytically. In this case, there is no preload scatter considered, so this analysis serves as a reference and is represented in Figure 15. Contrary to what happens in the case of axial load (see Figure 1), if the same value of the effective preload is considered for all the balls, the drop in the friction torque is not so pronounced. This happens because, under an applied bending moment, the load is not equally distributed among the balls. So even if the effective preload is the same for every ball, they change from the two-point state to the four-point state more progressively and not all at once for the same applied external load.

Table 4. Studied cases to analyse and compare the effect of the flexibility of the rings and surrounding structures on the load distribution and the friction torque.

TITLE	PRELOAD	LOAD DISTRIBUTION	FRICTION TORQUE
FEM-Analytical	FEM	FEM	Analytical
Analytical 1	FEM average	Analytical	Analytical
Analytical 2	FEM	Analytical	Analytical

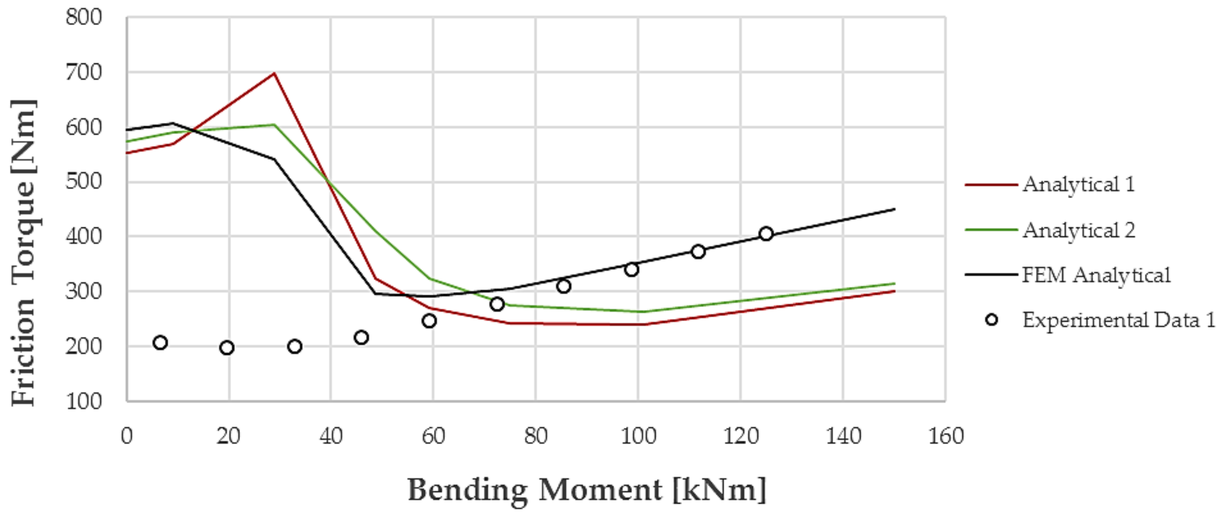

Figure 15. Friction torque analysis feeding analytical tool with different stages of *FE* data.

In the second analysis, which is named *Analytical 2*, the applied preload corresponds to the ball-raceway deformations extracted from the *FE* analysis after the first load step (see Figure 13), but considering each ball independently, and not applying the mean value, like in *Analytical 1*. Thus, this approach considers the different resulting ball loads on the individual raceways caused by the ring deformation after the first load step. Looking at the results of both *Analytical 1* and *Analytical 2* for high loads in Figure 15, it can be seen that both curves converge to the same results, which are near the ones in Figure 11b for the analytical approach. Due to that, and since in this load range the *FEM-Analytical* fits the test results, it is confirmed that the reason for the bad correlation between the analytical approach and the test results is that the flexibility of the structures is not being considered in the former model. If we look at low loads, the three curves are very far from the tests. This confirms that the ball preload scatter, which is not being considered in either case, plays a decisive role in this load range.

In conclusion, to achieve a good estimation of the friction torque for low bending moments, there are two options: (1) either the structures are rigid and the analytical approach can be applied, so the preload scatter can be considered as proposed in this work; or (2) the structures are so flexible that they affect the friction torque, as it is the case, and therefore the load distribution must be solved via FE analysis, considering also the preload scatter. Since many calculations are required considering different combinations of *m* and *SD*, and due to the high computational cost linked to FE simulations, the second option goes beyond the scope of this research work. Nonetheless, it will be studied in future work. A practical way to approach this future research may involve applying the superelement technique in order to avoid high computational costs.

In order to complete the study and justify the effect of the deformation of the rings on the friction torque, the results of the load distribution for an applied bending moment of 150kNm are presented in Figure 16, considering both rigid rings, according to the analytical model, and flexible rings, simulated via FE analysis. The figure also shows the contribution of each ball to the total friction torque, which is a function of the load distribution. For the sake of completeness, the contact angle is also given in the figure. The results in the figure are for the upper row of the lower bearing (see Figure 12).

Looking at the most loaded region, which takes place at 0° and 180° in Figure 16a, the balls are facing higher forces in the analytical model than in the FE model. This observation is coherent with previous publications [13,15,18,21]. These balls are in a two-contact point state and, as observed in Figure 16b, the higher the load, the higher the contribution to the friction torque is. If we look at the less loaded balls, located at 90° and 270°, they are in a four-point contact state, i.e. both contact diagonals are loaded (see the region coloured in grey). Contrary to observations in [13,15,18,21], considering the flexibility of the structures does not lead to more balls in the four-point contact zone in this case. Nonetheless, the balls with four-point contacts are more loaded according to the FE model, which leads to a higher value of friction torque. Figure 16b shows how, coherently with previous explanations based on Figure 2b, the contribution to the friction torque is higher for the balls in the four-point contact zone, even if they are less loaded. Therefore, and because the load in these balls is lower under the rigid rings assumption, the friction torque is also lower for the analytical model than for the FE model under the considered load of 150kNm.

This explains why the proposed analytical approach retrieves lower friction torque estimations than the experimental results in Figure 11b and Figure 15 for high loads. In the case of low loads, and as stated before, the friction torque is more conditioned by the preload, and therefore by its scatter.

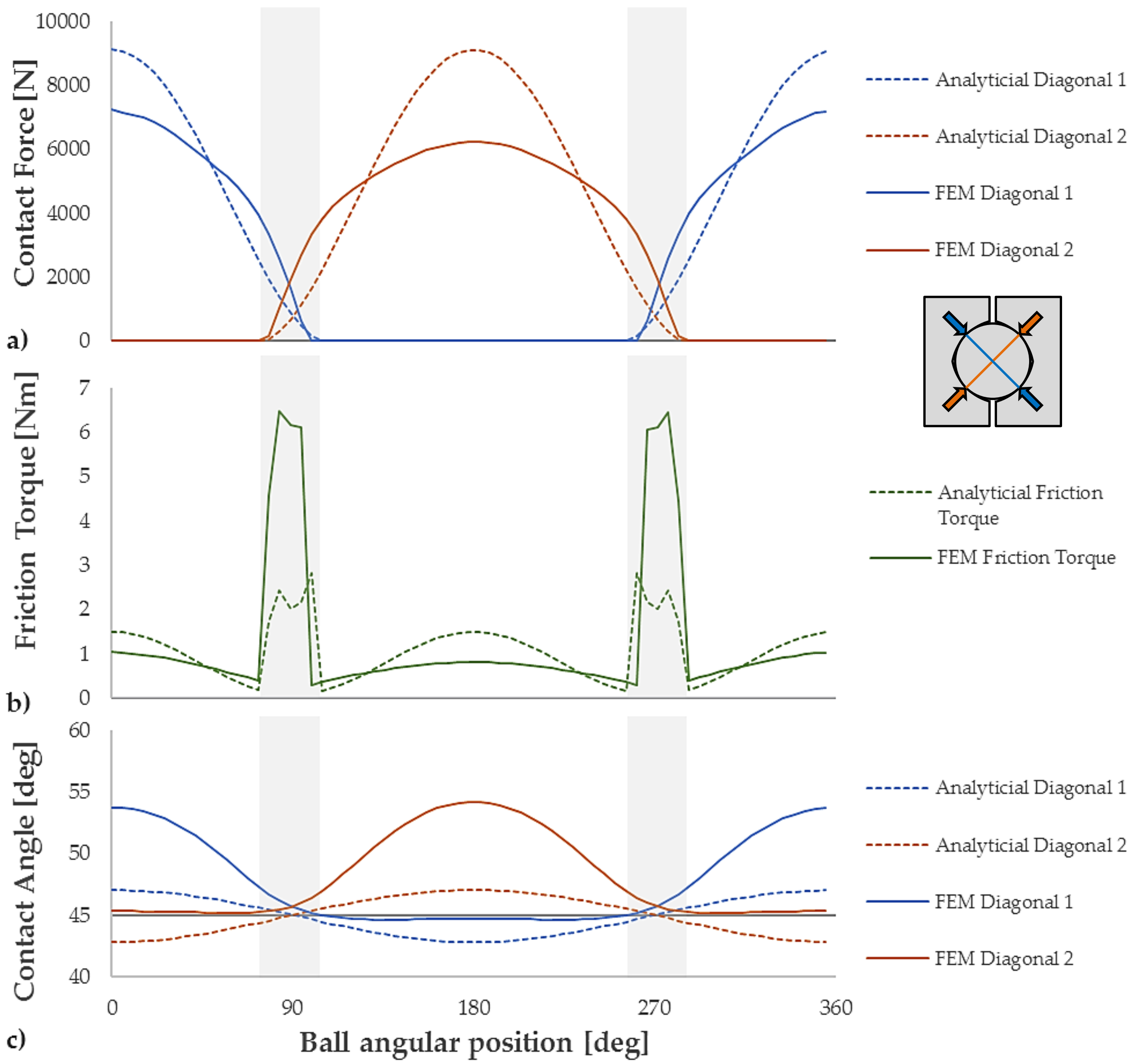

Figure 16. Load (a), friction torque (b) and contact angle (c) distribution for the analytical tool and FE simulations for a bending moment of 150kNm.

6. Guidelines for different case scenarios

The user of the proposed analytical approach may face different case scenarios while applying it to specific bearings. The available bearing data will vary depending if the user is a bearing manufacturer, a customer with some knowledge about the product, or a final user unaware of any technical data. Based on that, this section offers guidelines about how to use and tune the model in order to get the most reliable friction torque prediction tool possible. To this aim, three case scenarios are considered: the one studied in this manuscript (*Case 1*), the best-case scenario (*Case 2*) and the worst-case scenario

(*Case 3*). The cases are summarised in Table 5. Depending on the case, different data will be known. In this regard, the user may deal with the unknown data in two ways: either make assumptions (e.g. based on the bibliography or previous experience) or tune the model for their specific bearing by means of experimental tests, considering the unknown data as the tuning parameters. For the second strategy, this section proposes the minimum number of tests to be carried out. In this regard, the simplest tests are considered, i.e. in idling conditions or under an axial load.

Table 5. Considered case scenarios.

Scenario	**Known data**		**Unknown data**	
Case 1	Global geometry:	D_{pw}, i	Coefficient of friction:	μ
	Internal geometry:	D_w, z, α_0, s	Ball preload:	m, SD
			Independent constant:	C
Case 2	Global geometry:	D_{pw}, i	Ball preload (average):	m
	Internal geometry:	D_w, z, α_0, s	Independent constant:	C
	Coefficient of friction:	μ		
	Ball preload (scatter):	SD		
Case 3	Global geometry:	D_{pw}, i	Almost everything	

Of course, many other intermediate cases than the ones in Table 5 may take place in practice. In those cases, the user may adapt its strategy based on the case scenarios described below.

6.1. Case 1: Studied case

This would be the case for customers with access to the drawings of the bearing. It is the case studied in this manuscript indeed, so all the geometry data was known (see Section 2.4). The procedure to tune the model is the one described in Section 4.2, where a minimum of four test measurements would be required:

- Two measurements under high axial load: these points are necessary to determine μ, so they must be in the two-point contact zone (see Figure 9).
- Two measurements under low axial load: these points must be located in the four-point and/or the

transition zone. One of these points may correspond to an unloaded case. With these two points and the previous ones, the parameters *m*, *SD* and *C* can be set.

6.2. Case 2: Best-case scenario

This can be the case of a bearing manufacturer, not only with access to the data regarding the particular bearing to be characterized but also to previous experience and deep knowledge regarding their product, their manufacturing tolerances, previous test campaigns, etc. With all this information, the user can have access to reliable values for μ and *SD*. Of course, for the manufacturer, the geometry is also known. Therefore, the only unknowns would be *m* and *C*. In this case, the procedure to tune the model is easier, and the required minimum number of tests is lower:

- One measurement under high axial load to define the *C* parameter, since *m* has no effect in the two-point contact zone (see Figure 5b).
- One measurement in idling to define *m*.

6.3. Case 3: Worst-case scenario

This would be the case for a final user whose unique data is D_{pw}, since the geometry of the structure where the bearing is installed must be at least known in order to have some estimation of the friction torque. This is indeed the only data required by the formula proposed by the NREL [1].

In this case, only rough estimations can be made for the friction torque by using the proposed approach. To this aim, data from the bibliography can be considered for certain parameters like μ or *s*, but others can only be estimated, based on conservative assumptions. Having so little information, in this case, the formula from the NREL could be enough to obtain rough estimations for the most loaded case, but the results must be carefully interpreted, since it can retrieve non-conservative results for low loads.

7. Conclusions

The proposed analytical methodology calculates the friction torque in ball slewing bearings considering the ball preload scatter. This preload scatter has been proven as an effective way to smooth the abrupt transition that state-of-the-art analytical models show for an applied axial load. Moreover, it allows the model to achieve a successful correlation with experimental tests under compression loads. Nonetheless, and depending on the stiffness of the structures to which the bearing is assembled, the rigid ring assumption considered in the approach can lead to inaccurate friction torque results when a bending moment, or a tension load (less common), is applied.

An important additional conclusion is that, under an applied bending moment, the friction torque has been proven to be driven by the less loaded balls, which have four points in contact, and not by the most loaded ones, which have only two. This evidences how sensitive the friction torque is to the preload (and its scatter) even for high applied bending moments, since the higher the preload is, the more balls will be under the four-point contact state, and therefore the higher the friction torque will be.

The methodology described in this research work is meant to have a practical application, useful for users ranging from a bearing manufacturer with extensive knowledge about his product to a user with more limited information. Thus, the manuscript provides guidelines about how to use and tune the model to get a reliable friction torque prediction tool. In this sense, the presented analytical approach gives far more accurate results than the practical formula proposed by the NREL for this type of bearings, even if the latter can still be useful for rough estimations when only the global dimensions of the bearing are known.

To take into account the flexibility of the rings and the structures, the FEM has been proven an effective but not efficient way. Moreover, no simulations have been performed considering both the preload scatter and the flexibility of the structures. Therefore, the simulations performed in this research work with flexible structures offer good correlation with experimental results for high loads, but poor results for low loads, where the preload (and its scatter) has a great effect. The simulation of both the flexibility of the structures and the preload scatter can be performed efficiently by implementing the stiffness matrixes of the system in the analytical procedure. The authors will focus their future work on this line.

8. Acknowledgements

The authors would like to thank the Ministry of Economy and Competitiveness of the Spanish Government through the projects with grant number DPI2017-85487-R and PID2021-122746OB-I00 (MCIN/AEI/10.13039/501100011033 and FEDER Una manera de hacer Europa) and the Basque Government through the project with grant number IT1542-22 for their financial support. Furthermore, this research has been supported by the German Federal Ministry for Economic Affairs and Climate Action through the iBAC project with grant number 0324344A.

9. Competing interests

The authors have no competing interests to declare that are relevant to the content of this article.

10. References

[1] T.A. Harris, J.H. Rumbarger, C.P. Butterfield, Wind Turbine Design Guideline DG03: Yaw and Pitch Rolling Bearing Life. Technical Report: NREL/TP-500-42362, Golden, Colorado, 2009. https://www.nrel.gov/docs/fy10osti/42362.pdf.

[2] Schaeffler Technologies AG & Co. KG, Large Size Bearings Ball bearings Roller bearings Back-up rollers Spherical plain bearings Bearing housings Accessories, (2015). https://www.schaeffler.com/remotemedien/media/_shared_media/08_media_library/01_publications/schaeffler_2/catalogue_1/downloads_6/gl1_de_en.pdf (accessed December 15, 2022).

[3] Thyssenkrupp, Rothe Erde ® Slewing Bearings Catalogue, Dortmund, 2020. https://www.thyssenkrupp-rotheerde.com/en/downloads/brochures-and-catalogues/download (accessed December 15, 2022).

[4] L. Houpert, Ball bearing and tapered roller bearing torque: Analytical , numerical and experimental results, Tribol. Trans. (2002).

[5] SKF Group, Rolling bearings catalogue, PUB BU/P1 17000/1 EN. (2018) 1152. https://www.skf.com/group/products/rolling-bearings (accessed December 15, 2022).

[6] Timken, Timken Engineering Manual, 150 11-22 Order No. 10424. (2022).

https://www.timken.com/resources/timken-engineering-manual/ (accessed December 16, 2022).

[7] Y. Zhao, Z. Ma, Y. Zi, Skidding and spinning investigation for dry-lubricated angular contact ball bearing under combined loads, Frict. 2022. (2023) 1–21. doi:10.1007/S40544-022-0703-9.

[8] A.B. Jones, Ball Motion and Sliding Friction in Ball Bearings, J. Basic Eng. 81 (1959) 1–12. doi:10.1115/1.4008346.

[9] A. Leblanc, D. Nelias, Ball Motion and Sliding Friction in a Four-Contact-Point Ball Bearing, J. Tribol. 129 (2007) 801–808. doi:10.1115/1.2768079.

[10] A. Leblanc, D. Nelias, Analysis of Ball Bearings with 2, 3 or 4 Contact Points, Tribol. Trans. 51 (2008) 372–380. doi:10.1080/10402000801888887.

[11] A. Joshi, B. Kachhia, H. Kikkari, M. Sridhar, D. Nelias, Running Torque of Slow Speed Two-Point and Four-Point Contact Bearings, Lubricants. 3 (2015) 181–196. doi:10.3390/lubricants3020181.

[12] I. Heras, Four-point contact slewing bearings for wind turbines: advances in structural modelling and friction torque calculation, University of the Basque Country (UPV/EHU), 2018.

[13] I. Heras, J. Aguirrebeitia, M. Abasolo, Friction torque in four contact point slewing bearings: Effect of manufacturing errors and ring stiffness, Mech. Mach. Theory. 112 (2017) 145–154. doi:10.1016/j.mechmachtheory.2017.02.009.

[14] I. Heras, J. Aguirrebeitia, M. Abasolo, J. Plaza, Friction torque in four-point contact slewing bearings: Applicability and limitations of current analytical formulations, Tribol. Int. (2017). doi:10.1016/j.triboint.2017.05.011.

[15] I. Heras, J. Aguirrebeitia, M. Abasolo, I. Coria, I. Escanciano, Load distribution and friction torque in four-point contact slewing bearings considering manufacturing errors and ring flexibility, Mech. Mach. Theory. 137 (2019) 23–36. doi:10.1016/j.mechmachtheory.2019.03.008.

[16] J. Aguirrebeitia, R. Avilés, I. Fernández de Bustos, M. Abasolo, Calculation of General Static Load-Carrying Capacity for the Design of Four-Contact-Point Slewing Bearings, J. Mech. Des. 132

(2010) 64501–64506. doi:10.1115/1.4001600.

[17] J. Aguirrebeitia, J. Plaza, M. Abasolo, J. Vallejo, Effect of the preload in the general static load-carrying capacity of four-contact-point slewing bearings for wind turbine generators: theoretical model and finite element calculations, Wind Energy. 17 (2014) 1605–1621. doi:10.1002/we.1656.

[18] M. Olave, X. Sagartzazu, J. Damian, A. Serna, Design of four contact-point slewing bearing with a new load distribution procedure to account for structural stiffness, J. Mech. Des. Trans. ASME. 132 (2010) 0210061(10). doi:10.1115/1.4000834.

[19] A. Daidié, Z. Chaib, A. Ghosn, 3D Simplified Finite Elements Analysis of Load and Contact Angle in a Slewing Ball Bearing, J. Mech. Des. 130 (2008) 82601. doi:10.1115/1.2918915.

[20] J. Aguirrebeitia, M. Abasolo, R. Avilés, I. Fernández de Bustos, General static load-carrying capacity for the design and selection of four contact point slewing bearings: Finite element calculations and theoretical model validation, Finite Elem. Anal. Des. 55 (2012) 23–30. doi:10.1016/j.finel.2012.02.002.

[21] G. Chen, J. Wen, Load performance of large-scale rolling bearings with supporting structure in wind turbines, J. Tribol. 134 (2012). doi:10.1115/1.4007349.

[22] R. Liu, H. Wang, B.T. Pang, X.H. Gao, H.Y. Zong, Load distribution calculation of a four-point-contact slewing bearing and its experimental verification, Exp Tech. 42 (2018) 243–252. doi:10.1007/s40799-018-0237-2.

[23] M. Krynke, R. Ulewicz, ScienceDirect ScienceDirect Analysis of the influence of slewing bearing mounting on their static load capacity, (2019). doi:10.1016/j.trpro.2019.07.105.

[24] S. Leupold, R. Schelenz, G. Jacobs, Method to determine the local load cycles of a blade bearing using flexible multi-body simulation, Forsch. Im Ingenieurwesen/Engineering Res. 85 (2021) 211–218. doi:10.1007/S10010-021-00457-Y/FIGURES/9.

[25] D. Becker, D. Billenstein, T. Handreck, P. Müller, M. Neidnicht, G. Volmer, D. Schlüter, T. Netz, B. Lüneburg, J. Rollmann, Design and calculation process for large-sized multi-MW blade

bearing applications based on advanced multi-bearing FE-analyses, Bear. World Int. Conf. (2022) 280–284.

[26] M. Buescher, R. Schelenz, G. Jacobs, V. Schneider, G. Poll, Contact Analysis of Wind Turbine Blade Bearings by Means of Finite Element Method and Alternative Slicing Technique Contact Load Modeling, Bear. World Int. Conf. (2022) 286–294.

[27] M.S. Starvin, K. Manisekar, The effect of manufacturing tolerances on the load carrying capacity of large diameter bearings, Sadhana. 40 (2015) 1899–1911.

[28] S. Aithal, N. Siva Prasad, M. Shunmugam, P. Chellapandi, Effect of manufacturing errors on load distribution in large diameter slewing bearings of fast breeder reactor rotatable plugs, Proc. Inst. Mech. Eng. Part C J. Mech. Eng. Sci. 230 (2016) 1449–1460. doi:10.1177/0954406215579947.

[29] M.R. Lovell, M.M. Khonsari, R.D. Marangoni, Low-Speed Friction Torque on Balls Undergoing Rolling Motion, Tribol. Trans. (1993) 290–296.

[30] L. Houpert, Numerical and analytical calculations in ball bearings, in: 8th Eur. Sp. Mech. Tribol. Symp. Vol. 438, Toulouse, France, 1999: p. 283. https://ui.adsabs.harvard.edu/abs/1999ESASP.438..283H.

[31] T. Cousseau, B. Grac -A A, A. Campos, J. Seabra, Friction torque in grease lubricated thrust ball bearings, (2010). doi:10.1016/j.triboint.2010.06.013.

[32] D. Gonçalves, S. Pinho, B. Graça, A. V Campos, J.H.O. Seabra, Friction torque in thrust ball bearings lubricated with polymer greases of different thickener content, Tribol. Int. 96 (2016) 87–96. doi:10.1016/j.triboint.2015.12.017.

[33] C. Long, X. Xintao, Z. Haotian, Q. Ming, Friction Torque Behavior as a Function of Actual Contact Angle in Four-point-contact Ball Bearing, Appl. Math. Nonlinear Sci. 1 (2016) 53–64. doi:10.21042/AMNS.2016.1.00005.

[34] I. Heras, I. Coria, J. Aguirrebeitia, M. Abasolo, I. Martín, Par de fricción en rodamientos de vuelco de cuatro puntos de contacto: procedimiento de cálculo y resultados experimentales, in: XXII

Congr. Nac. Ing. Mecánica, 19-21 Sept., Madrid, Spain, 2018.

[35] M. Stammler, F. Schwack, N. Bader, A. Reuter, G. Poll, Friction torque of wind-turbine pitch bearings – comparison of experimental results with available models, Wind Energy Sci. 3 (2018) 97–105. doi:10.5194/wes-3-97-2018.

[36] O. Menck, K. Behnke, M. Stammler, A. Bartschat, F. Schleich, M. Graßmann, Measurements and modeling of friction torque of wind turbine blade bearings, J. Phys. Conf. Ser. 2265 (2022) 022087. doi:10.1088/1742-6596/2265/2/022087.

[37] N. De Laurentis, A. Kadiric, P. Lugt, P. Cann, The influence of bearing grease composition on friction in rolling/sliding concentrated contacts, Tribol. Int. 94 (2016) 624–632. doi:10.1016/J.TRIBOINT.2015.10.012.

[38] J. Guegan, A. Kadiric, A. Gabelli, H. Spikes, The Relationship Between Friction and Film Thickness in EHD Point Contacts in the Presence of Longitudinal Roughness, Tribol. Lett. 64 (2016) 1–15. doi:10.1007/S11249-016-0768-6/FIGURES/21.

[39] L. Yang, W. Xue, S. Gao, H. Liu, Y. Cao, D. Duan, D. Li, S. Li, Study on sliding friction and wear behavior of M50 bearing steel with rare earth addition, Tribol. Int. 174 (2022) 107725. doi:10.1016/J.TRIBOINT.2022.107725.

Author biography

Iñigo Escanciano. He is currently a Ph.D. candidate in mechanical engineering in the University of the Basque Country, Bilbao, Spain. As part of the Mechanical Analysis and Design research group, his research consists on the simulation and analysis of ball slewing bearings. He received his B.Sc. degree in mechanical engineering in 2016 in the University of the Basque Country, Spain. Since then until today he has been part of the ESI Bilbao MotoStudent team at the University of the Basque Country, where he received his M.Sc. degree in mechanical engineering in 2018.

Graphical abstract